Chapter

Plasma-Enabled Dry Methane Reforming

Zunrong Sheng, Seigo Kameshima, Kenta Sakata and Tomohiro Nozaki

Abstract

Plasma-enabled dry methane reforming is a promising technology for biogas upgrade and shows multiple benefits to provide additional energy and material conversion pathways. This chapter first presents the role of nonthermal plasma as a potential energy supply pathway in the low-temperature methane conversion: an appropriated combination of electrical energy provided by plasma (ΔG) and the low-temperature thermal energy ($T\Delta S$) satisfies the overall reaction enthalpy (ΔH) with higher energy conversion efficiency. Moreover, plasma-enabled dry methane reforming could be operated at much lower temperature than thermal catalysis with sufficient material conversion. Three kinds of typical packed-bed plasma reactor were introduced to give a better understanding of the application of plasma and catalyst hybrid system. Subsequently, plasma-enabled dry methane reforming was diagnosed by pulsed reaction spectrometry compared with thermal catalysis, presenting a clear overview of gas component changes and significant promotion in reactant conversion and product yield. The interaction between plasma and catalyst was summarized based on two aspects: catalyst affects plasma, and plasma affects catalyst. We discussed the coke formation behavior of Ni/Al_2O_3 catalyst in the plasma-enabled and thermal dry methane reforming, followed by the oxidation behavior. The interaction between plasma and catalyst pellets was discussed toward deeper insight into the mechanism.

Keywords: plasma catalysis, dry methane reforming, dielectric barrier discharge, biogas, methane conversion

1. Introduction

Dry methane reforming (DMR) has drawn keen attention as viable CO_2 utilization technology because it may have one of the greatest commercial potentials [1, 2].

$$CH_4 + CO_2 \rightarrow 2H_2 + 2CO \quad \Delta H = 247\ \text{kJ/mol} \qquad \text{(R1)}$$

Moreover, products are the main components of syngas (H_2 and CO), which can be converted to the synthetic fuels as well as H_2 carrier via well-established C1 chemistry. Conventionally, the H_2/CO ratio from DMR is more suitable for Fischer-Tropsch synthesis than other methane reforming reactions [3–5]. **Figure 1** shows the reaction enthalpy and Gibbs free energy of DMR (R1) with respect to temperature. According to the definition, reaction enthalpy (Eq. (1)) consists of two terms:

$$\Delta H = T\Delta S + \Delta G \qquad (1)$$

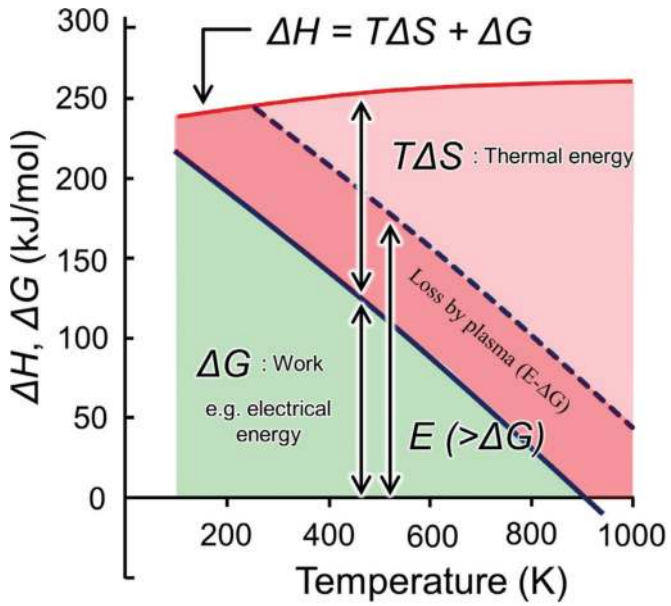

Figure 1.
Energy diagram of DMR.

DMR is categorized as uphill (endothermic) reaction where energy input (ΔH) is indispensable in order to satisfy the conservation of energy. Moreover, the reaction does not occur spontaneously by the low-temperature thermal energy due to the large positive value of ΔG at low temperature. **Figure 1** shows that at least 900 K is required to have a negative value of ΔG, and all energy is supplied via high-temperature thermal energy. Such high-temperature heat is supplied by the combustion of initial feed that produces CO_2 as well as NO_x. Net CO_2 utilization is partly canceled unless combustion-generated CO_2 is utilized which is economically quite difficult. Moreover, heat transfer from the combustion gas flowing outside of the reactor to the catalyst bed governs the overall material throughput which is known as a *heat transfer-limiting* regime. Because the heat transport property of a fixed bed reactor is poor, excessively high-temperature operation beyond thermodynamic limitation (i.e., 900 K) is necessary.

To overcome the aforementioned problem, low-temperature DMR is demanded, pursuing a new technology, and potential use of nonthermal plasma is highlighted. Assume DMR is operated at a lower temperature than the thermodynamic limitation as schematically depicted in **Figure 1**. A part of the energy is supplied by a low-temperature thermal energy ($T\Delta S$), while the rest of energy is supplied by the electricity (ΔG) under the nonthermal plasma environment so that $T\Delta S + \Delta G$ satisfies reaction enthalpy (ΔH). Electrical energy is used to accelerate electrons; subsequently, the electron energy is transferred to the molecules to initiate DMR at much lower temperature than thermal catalysis. Electronic collision process is independent of reaction temperature if gas density does not change significantly. Meanwhile, a part of the electrical energy is converted to heat: electrical energy consumed by nonthermal plasma (E) is depicted in the dashed line in **Figure 1**: inevitably, E is greater than ΔG at a fixed temperature. Although heat generated by nonthermal plasma is considered as energy loss (i.e., $E-\Delta G$), both excited species and heat are utilized via endothermic DMR, which enables efficient use of electrical energy without *heat transfer limitation*: electrification of reforming reaction, or chemical processes in general, has the greatest advantage that the energy transfer and the control are independent of temperature gradient.

Dielectric barrier discharge (DBD) is the most successful atmospheric pressure nonthermal plasma sources in industry applications [6] and is used exclusively for this purpose. DBD is combined with a catalyst bed reactor and generated at atmospheric pressure [7]. DBD is characterized as a number of transient discharge channels known as streamers with nanosecond duration. Because the streamer has a nature of propagation along the interface between two adjacent dielectric materials, namely, the catalyst pellet and the gas interface, excited species produced by DBD is transferred to the catalyst surface efficiently. Moreover, the heat generated by DBD is transferred directly to the catalysts; overall energy transfer from nonthermal plasma to the catalyst bed is efficient. If the electricity is supplied from the renewable energy such as photovoltaics and wind turbines, low-emission DMR is possible with free of combustion. Moreover, nonthermal plasma-assisted C1 chemistry enables renewable-to-chemical energy conversion, which provides an alternative and viable solution for the efficient renewable energy storage and transportation pathways.

The aforementioned thermodynamic analysis (**Figure 1**) implies that the temperature-benign and low-emission chemical processes are possible with the appropriate combination of nonthermal plasma and the heterogeneous catalysts. Meanwhile, such hybrid system does not work at room temperature simply because the overall reaction rate is *kinetically controlled* at much low temperature: Nevertheless, we would like to highlight that nonthermal plasma technology solves many technological obstacles such as the elimination of combustion as well as heat transfer limitation. Moreover, low-temperature operation suppresses coke formation which is one of the big issues in DMR. In this book chapter, we focus on low-temperature DMR and compare thermal and plasma catalysis. Plasma catalysis of DMR was diagnosed by pulsed reaction spectrometry [8], and results were compared with thermal catalysis to highlight the benefit of DBD and catalyst combination. Subsequently, the interaction between DBD and catalyst pellets was discussed toward deeper insight into the mechanism. Finally, future prospects of plasma catalysis of DMR are provided.

2. Packed-bed plasma reactor

Based on the location and number of plasma zone and catalyst bed, the combination of heterogeneous catalysts with plasma can be operated in three configurations: single-, two- and multistage, which are shown in **Figure 2**.

2.1 Single-stage reactor

In a single-stage reactor (**Figure 2(a)**), the catalyst is packed inside the plasma zone, where the interaction of plasma and catalysts occurs. Because thermal plasma (gas bulk temperature >3000°C [9]) could damage catalyst, single-stage reactor is, therefore, suitable for nonthermal plasma sources. The single-stage reactor is widely applied in CH_4 reforming [10–14], direct conversion of CO_2 [15–19], VOCs abatement [20–22], exhaust matter removal [23], formaldehyde removal [24], NO_x synthesis [25], and ozone synthesis [6]. There are two significant merits of single-state reactor: (I) great flexibility exists in terms of electrode and reactor configurations that the reactor can be constructed using inexpensive materials such as glass and polymers and (II) reactive species, ions, electrons, etc. generated by nonthermal plasma could modify the gas composition, which affects the surface reactions with catalyst synergistically. However, the interaction between plasma and catalyst is complex when the catalyst is placed directly in the plasma zone. The synergy of plasma and catalyst will be discussed further in Section 4 based on the single-state reactor.

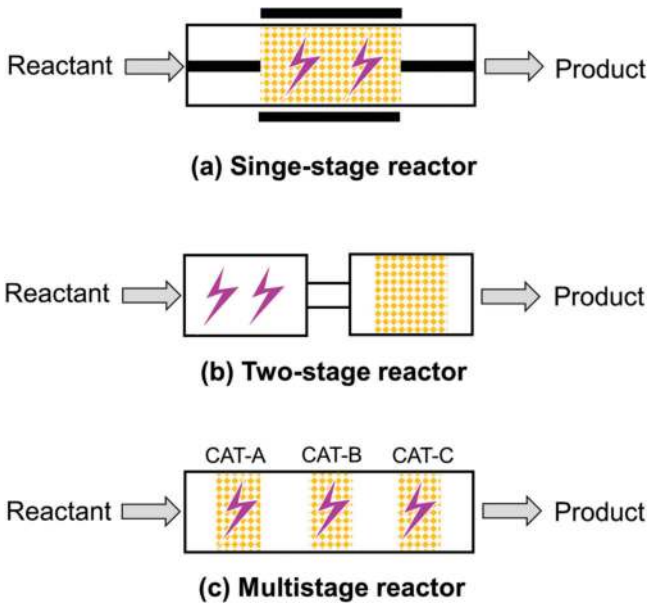

Figure 2.
Schematic diagram of single-stage (a), two-stage (b), and multistage reactor (c). Catalyst is depicted as orange circle; plasma is depicted as purple "lightning" symbol.

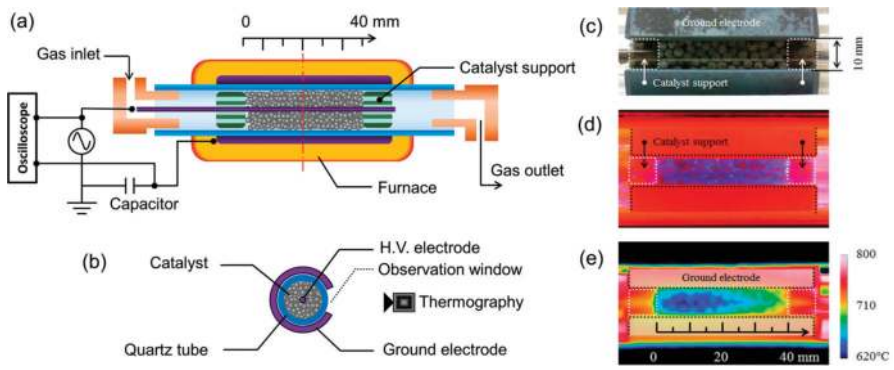

Figure 3.
Single-stage DBD reactor system for DMR: (a) overview of the reactor system, (b) cross-sectional view, (c) overview of the catalyst bed, (d) DBD generated in the catalyst bed, and (e) temperature distribution during reforming reaction.

Figure 3 depicts a single-stage DBD reactor for CH_4 reforming [26], mainly including a quartz tube reactor, high voltage (HV) electrode at the center, and ground electrode outside of the tube. Catalyst pellets are packed in the plasma zone between two electrodes, and both ends of the catalyst bed are fixed by metallic supports. The high voltage is applied between the HV centered electrode and ground electrode to generate dielectric barrier discharge over the pellet surface. Discharge power was measured by voltage-charge Lissajous analysis. The discharge gap, which is the distance between HV electrode and the ground electrode, is usually less than 10 mm [27]. Catalyst temperature is controlled by a furnace. The temperature distribution of the catalyst bed is measured by thermography through the observation window. **Figure 3(c)–(e)** shows an overview of the catalyst bed, DBD generated in the catalyst bed, and the temperature distribution during reforming reaction. The

catalyst bed temperature was clearly decreased because of the endothermic nature of DMR. In addition, gas temperature was estimated by optical emission spectroscopy (OES) of CO(B-A) transition [28], showing that catalyst temperature and gas temperature matched within a measurement error.

2.2 Two-stage reactor

In the two-stage reactor, the catalyst is located at the downstream of plasma (**Figure 2(b)**). The gas is first addressed by the plasma and subsequently interacts with the catalyst [29]. Due to the separation of plasma and catalyst, both thermal and nonthermal plasma can be utilized. Because excited species generated in plasma have very short lifetimes, plasma mainly plays the role to preconvert the gas composition and then feed it into the catalyst reactor, e.g., in NO_x removal process, due to the pretreatment of plasma, NO and NO_2 were coexisted, which enhanced the following selective catalytic reduction in catalyst bed [30]; the other example is the benzene removal process where ozone (O_3) was formed from background O_2 by plasma, which promoted the decomposition of benzene in the next stage [31]. However, compared with the single-stage reactor, application of a two-stage reactor is limited in plasma catalysis and shows a lower performance for a given catalyst [32–37].

2.3 Multistage reactor

The multistage reactor can be described as a combination of more than one single-stage bed/reactor (**Figure 2(c)**). The multistage reactor gives a more flexible option in the industrialization of the plasma catalysis, attributing to the combination of catalysts with a different function for the expected reaction [38]. Chavade et al. [39] used a four-stage plasma and catalytic reactor system for oxidation of benzene. The results showed that the increase in stage number enhanced benzene conversion and CO_2 selectivity. The same result can be found in biogas reforming process using a multistage gliding arc discharge system without catalyst [40]. Harling et al. [41] developed a three-stage reactor for VOCs removal. The combination of plasma and catalyst in series could significantly improve the efficiency of VOCs decomposition. At the same time, the formation of by-product such as NO_x was suppressed.

3. DBD-enabled dry methane reforming

The pulsed reaction spectrometry using DBD with Ni/Al_2O_3 catalysts was investigated to develop a reforming diagnostic method [10]. Pulsed reforming enables the transient analyses of both CH_4/CO_2 consumption and H_2 and CO generation. Furthermore, carbon formation was analyzed quantitatively without serious catalyst deactivation. The varied CH_4/CO_2 ratios between 0.5 and 1.5 were investigated at a fixed catalyst temperature near 600°C. The CH_4/CO_2 ratio was initially set to 0.5, and then the CH_4/CO_2 ratio was incremented stepwise until $CH_4/CO_2 = 1.5$, consecutively, while total flow rate was fixed at 1000 cm^3/min. De-coking process (R2) was followed up after every pulsed reaction. System pressure was kept at 5 kPa during the reforming process. Discharge power was 85–93 W where specific energy input was ca. 1.2 eV/molecule. Commercially available catalyst pellets (11 wt% $Ni\text{-}La/Al_2O_3$, Raschig ring type: 3 mm) was packed for 40 mm length (total weight ca. 12 g; Ni 1.36 g; La 0.35 g). **Figure 4** provides an overview of gas component changes in the entire hybrid reforming.

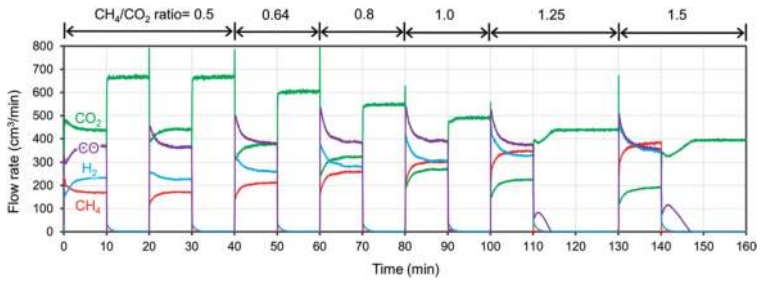

Figure 4.
Overview of the entire pulsed hybrid DMR.

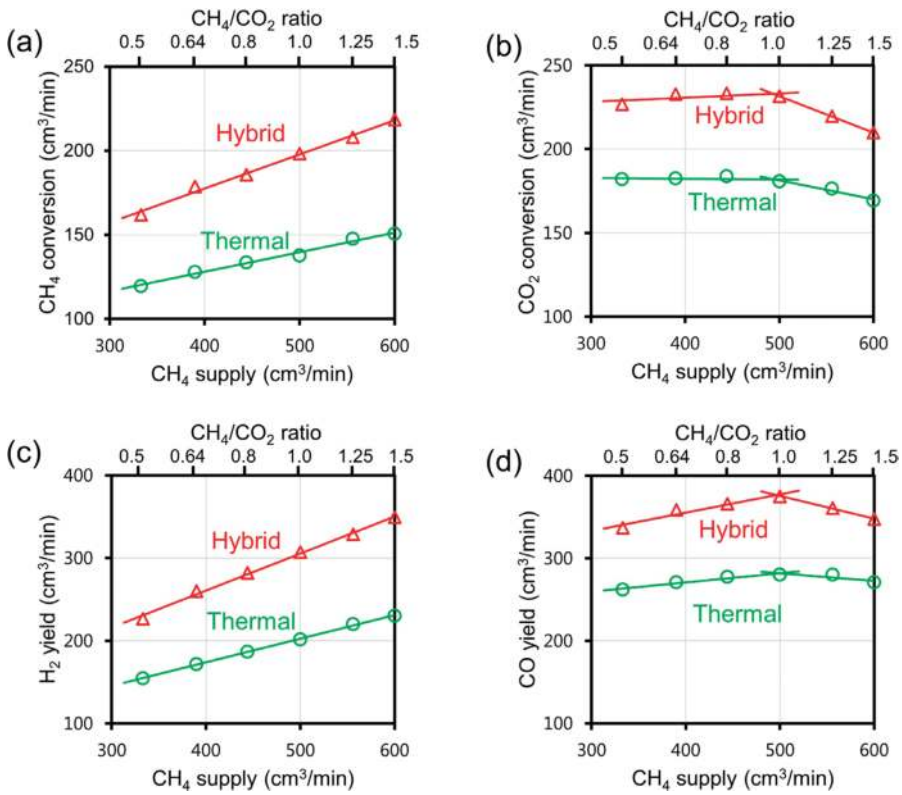

Figure 5.
Effects of CH_4/CO_2 ratio on DMR at ca. 600°C: (a) CH_4 conversion, (b) CO_2 conversion, (c) H_2 yield, and (d) CO yield.

Reactant conversion and product yields are shown in **Figure 5**. The definition for conversion and yield were provided in Ref. [8]. CH_4 conversion and H_2 yield were monotonically increased with the CH_4/CO_2 ratio. There are two simultaneous routes for CH_4 conversion as shown in **Figure 6**. Route (I) is a reforming path: CH_4 is chemisorbed on metallic sites (adsorbed species are denoted by * in reaction). The adsorbed CH_4 fragments (CH_x*) is oxidized by CO_2* to form CH_xO* before complete dehydrogenations to C* occurs. In route (II), CH_4 almost irreversibly dehydrogenates toward carbon atom, and then C*-rich layer is oxidized slowly by CO_2* (R2), which can be evidenced in the de-coking process in **Figure 4**. When the CH_4/CO_2 ratio exceeded 1.0, CH_4 prefers to dehydrogenate to solid carbon through route (II) due to the low proportion of CO_2. Subsequently, a nonnegligible amount of solid carbon is produced, and CO_2 conversion and CO yield turned to proportionally decrease.

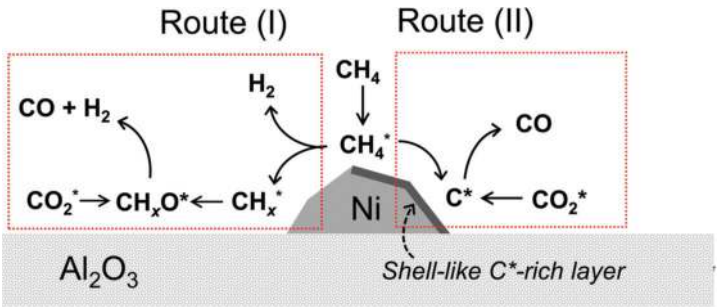

Figure 6.
Two simultaneous routes for CH_4 conversion.

$$C + CO_2 \rightarrow CO + CO \quad \text{(R2)}$$

$$CH_4 \rightarrow CH_4^* \rightarrow CH_x^* + \frac{(4-x)}{2} H_2 \; (x = 0\text{–}3) \quad \text{(R3)}$$

$$H_2 + CO_2 \rightarrow CO + H_2O \quad \text{(R4)}$$

$$C + H_2O \rightarrow H_2 + CO \quad \text{(R5)}$$

Compared with thermal reforming, both CH_4 conversion and H_2 yield were clearly promoted in hybrid reforming (**Figure 5**), and the main pathway of CH_4 conversion and H_2 yield could be simply described as CH_4 dehydrogenation (R3). It is proposed that CH_4 dehydrogenation was enhanced by the synergistic effect of DBD and catalyst. Molecular beam study revealed that dissociative chemisorption of CH_4 on the metal surface was enhanced by vibrational excitation [42]. The numerical simulation of one-dimensional streamer propagation demonstrated that the vibrationally excited CH_4 is the most abundant and long-lived species generated by low-energy electron impact [43]. The reaction mechanism of plasma-enabled catalysis could be explained by the Langmuir-Hinshelwood (LH) reaction scheme. The analysis of overall activation energy is expected to understand the contribution of plasma-generated reactive species.

The CO_2 conversion and CO yield were promoted in hybrid reforming compared to thermal reforming (**Figure 5**). H_2O was simultaneously produced as a by-product by reverse water gas shift (RWGS) reaction (R4). Reactivity of plasma-activated H_2O was confirmed by Arrhenius plot analysis where reaction order for H_2O was doubled by DBD [44]. Plasma-activated H_2O promotes reaction with adsorbed carbon; it creates additional pathways (R5) to syngas (H_2 and CO). The CO_2 conversion and CO yield were promoted in the hybrid reforming, illustrating that the reverse-Boudouard reaction (R2) was enhanced by DBD. The reaction between plasma-activated CO_2 and adsorbed carbon increases CO yield. The same result was obtained in the de-coking period [10]. Although excessive production of carbon is detrimental for catalyst activity and lifetime, the presence of adsorbed carbon creates key pathways for emerging plasma-induced synergistic effect. Consequently, plasma-activated CO_2 and H_2O would promote surface reaction and increase CO and H_2 yield. **Figure 5** clearly shows that the slope of each line increased in hybrid reforming compared with thermal reforming, attributing to the nonthermal plasma-excited species. The increase of slope

could be further explained by the promoted overall reaction order, which plays the key role in the estimation of the rate-determining step [44].

4. The synergy of plasma and catalyst

Synergism in plasma catalysis in the single-stage reactor is not fully understood due to the complex interaction between the various plasma-catalyst interaction processes [45–49]. Kim et al. [27] discussed the criteria for interaction between nonthermal plasma and the porous catalyst. The chemical species in nonthermal plasma are highly reactive; the lifetime is very short, e.g., O (^{1}D), 10 ns; O (3P), 50 μs; and OH, 100 μs: their one-dimensional diffusion length is limited from 0.7 to 65 μm. Plasma generated species within diffusion length from the external surface of pellets would contribute to the plasma-induced reaction pathways. The interdependence of plasma and catalyst can be discussed as two aspects: catalyst affects plasma, and plasma affects catalyst.

4.1 The effects of catalyst on plasma

With the packed catalyst in the plasma zone, gaseous species adsorbed on the catalyst surface increase the concentration of surface species. In addition, the electric field is enhanced near the catalyst surface due to catalyst nanofeatures [50, 51]. Moreover, the packed catalyst also enables the discharge type change, as well as microdischarge generation.

Without packed materials, discharge mode is the "free-standing" filamentary discharge propagating across the gas gap (**Figure 7(a)**). With a packed catalyst,

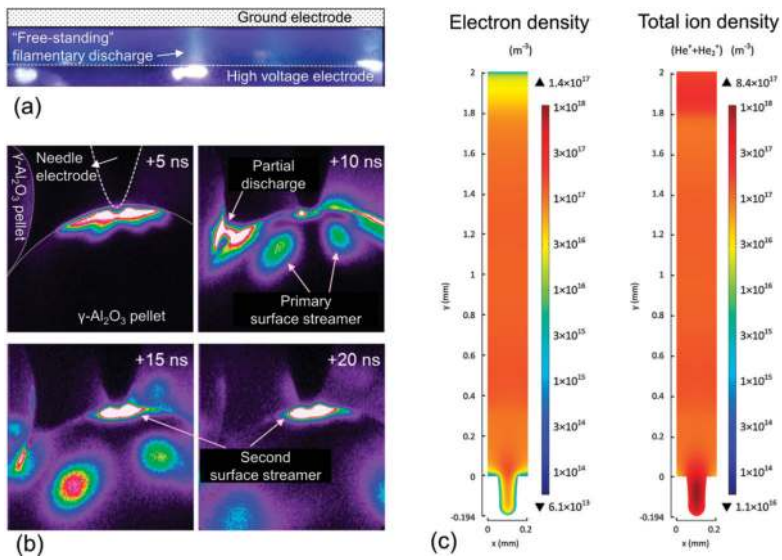

Figure 7.
(a) Filamentary discharge without catalyst pellet, (b) time-resolved images of surface streamers propagating on the surface of γ-Al_2O_3 (reproduced with permission from ref 54. Copyright 2016 IOP Publishing), and (c) distributions of the electron density and total ion density with a 100 μm pore (reproduced with permission from ref 56. Copyright 2016 Elsevier).

the surface streamer is propagated with the close contact with the catalyst surface, and intensive partial discharges occur between the contact area of catalysts [52, 53]. The time-resolved visualization of surface streamer propagation and partial discharge were detected by Kim et al. [54] with an intensified charge-coupled device (ICCD) camera. **Figure 7(b)** shows time-resolved images of surface streamers (i.e., primary surface streamer and secondary surface streamer) propagating on the surface. Enhanced catalytic performance in the presence of a catalyst is closely linked with the propagation of surface streamers [55]. Moreover, with packed catalyst, microdischarge is generated inside catalyst pores (when the pore sizes >10 μm) [56, 57]. Zhang et al. [56] investigated microdischarge formation inside catalyst pores by a two-dimensional fluid model in the μm range (**Figure 7(c)**), indicating that the plasma species can be formed inside pores of structured catalysts in the μm range and affect the plasma catalytic process.

4.2 The effects of plasma on catalyst

The plasma also affects the catalyst properties, which are summarized as the following aspects:

(I) Modification of physicochemical properties of the catalyst by plasma, which is widely used in catalyst preparation processes [58]. With plasma preparation, the catalyst obtains a higher adsorption capacity [59], higher surface area, and higher dispersion of the catalyst material [60–62], leading to a plasma-enhanced reactivity.

(II) It is possible that plasma makes changes in the surface process with the catalyst. As for the CH_4 reforming process, the deposited carbon from Ni catalysts can be removed effectively by plasma-excited CO_2 and H_2O [8]. The other example of the synergism is NH_3 decomposition for the application of fuel cell, where NH_3 conversion reached 99.9% when combining plasma and catalyst, although the conversion was less than 10% in the case of either plasma or catalyst only reaction [63].

(III) Based on Arrhenius plot analysis, plasma can decrease the activation barriers (overall activation energy), attributed to the vibrational excitation, which is schematically depicted in **Figure 8**. The net activation barrier will be $\left(E_a^{v=0} - E_{vib}\right)$ in an adiabatic barrier crossing case and $\left(E_a^{v=0} - E_{vib} - E^*\right)$ in a nonadiabatic barrier crossing case, respectively [64]. The activation barrier decrease was reported in toluene destruction process [65]. In steam methane reforming, the preexponential factor was increased clearly by plasma, attributing to plasma-activated H_2O removes adsorbed carbon species, which regenerate active sites for subsequent CH_4 adsorption [11].

(IV) The excited species or dissociated species might create other pathways with the presence of catalyst, e.g., during the CO_2 plasma oxidation process, plasma-enhanced CO_2 oxidized Ni/Al_2O_3 catalyst to form a NiO layer, which could drive an oxidation–reduction cycle in dry methane reforming reaction. The same NiO layer was found when specific energy input (*SEI*) was sufficiently high: the O_2 that dissociated from CO_2 plays the key role in the oxidation process. The details will be interpreted in Section 5.2.

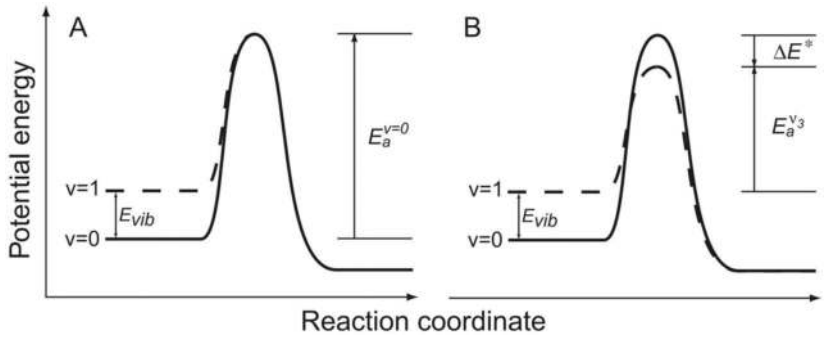

Figure 8.
Reduction of the overall activation energy by vibrational excitation of the reactants. (A) Adiabatic barrier crossing case and (B) nonadiabatic barrier crossing case. Reprinted with permission from ref 64. Copyright 2004 AAAS.

5. Discussion

5.1 Coke formation behavior

Coke formation behavior was studied as a reaction footprint to track reaction pathways induced by DBD [26]. Coke morphology and their distribution over the 3 mm spherical Ni/Al_2O_3 catalyst pellets were obtained after 60 min DMR. **Figure 9** shows cross-sectional carbon distribution, where (a)–(c) and (d)–(f) correspond to plasma catalysis and thermal catalysis in low, middle, and high temperatures. For the thermal catalysis with the temperature at 465°C, carbon deposition over the entire cross-section was obvious. With the temperature increased, coke was decreased and finally became nondetectable at ca. 620°C. At low temperature, plasma catalysis suppressed the coke formation significantly over the entire cross-section.

By the analysis of scanning electron micrographs (SEM) and Raman spectrum, fine carbon filaments were detected on the external pellet surface in plasma catalysis [26]. In contrast, thick fibrous carbon deposition was observed on the external surface in thermal catalysis, as well as in the internal pores in both thermal and plasma

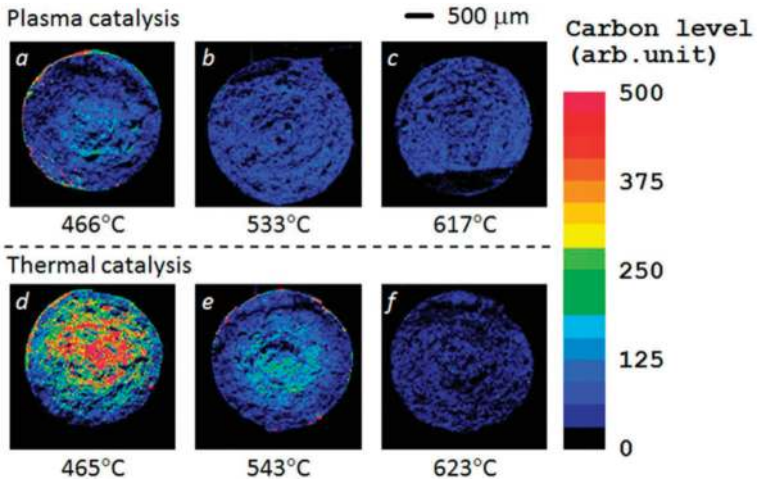

Figure 9.
Carbon distribution over the 3 mm spherical pellet cross-section after 60 min reforming: plasma catalysis (a)–(c) and thermal catalysis (d)–(f), respectively. Reprinted with permission from ref 26. Copyright 2018 IOP Publishing.

catalyses. The CH_4 dehydrogenation on catalyst is enhanced by nonthermal plasma, contributing to the generation of highly filamentous and amorphous carbon. Such nonthermal plasma-enhanced reaction has been demonstrated by carbon nanotube growth [66] and plasma-enabled steam methane reforming [67]. The fine amorphous carbon filaments, deposited in the external surface of catalyst, prove that the interaction of DBD occurs mainly in the external surface. Consequently, DBD generation and plasma-excited species diffusion are inhibited in the internal pores of catalyst.

5.2 Oxidation behavior of Ni/Al_2O_3 catalyst

The nickel (Ni) of Ni/Al_2O_3 catalyst was oxidized slightly by CO_2 in the thermal catalysis [68, 69] . However, the significant Ni oxidation by CO_2 (R6) was demonstrated when the catalyst were packed in nonthermal plasma zone. In this case, Ni uptakes surface oxygen beyond the adsorption/desorption equilibrium (i.e., Langmuir isotherm) to form NiO, which further promotes CH_4 dehydrogenation without solid carbon deposition (R7):

$$Ni + CO_2 \rightarrow NiO + CO \tag{R6}$$

$$NiO + CH_4 \rightarrow Ni + OH + CH_3 \tag{R7}$$

The specific energy input (*SEI*) is a critical operational parameter in plasma-enabled CO_2 treatment process due to the fact that dominant reaction pathway shifts dramatically with *SEI*:

$$SEI = C \times \frac{Discharge\ power\ (\mathrm{W})}{Total\ flow\ rate\ (\mathrm{cm^3/min})}\ (\mathrm{eV/molecule}) \tag{2}$$

SEI expresses energy consumption by discharging per unit volume of the feed gas, which could be further interpreted as average electrical energy (eV) per molecule. In Eq. (2), *C* is the conversion factor of the unit [10]. Two contrasting conditions are demonstrated in plasma-enabled CO_2 oxidation: one is designated as the direct oxidation route; with a small *SEI*, CO_2 dissociation to CO and 0.5 O_2 (R9) is negligible, and then the plasma-excited CO_2 dominates the oxidation process (R8). The other is the indirect oxidation route where O_2 provides an additional oxidation pathway; with a large *SEI*, CO_2 is dissociated into CO and O_2 (R9) without heterogeneous catalysts by electron impact [70, 71], followed by Ni oxidation by O_2 (R10).

$$\text{Direct oxidation route: } Ni + CO_2 \rightarrow NiO + CO \tag{R8}$$

$$\text{Indirect oxidation route: } CO_2 + e \rightarrow 1/2\ O_2 + CO + e \tag{R9}$$

$$Ni + 1/2\ O_2 \rightarrow NiO \tag{R10}$$

The plasma-enhanced direct oxidation route (R8) is further investigated because the plasma-enabled synergistic effect was demonstrated distinctly without O_2 [8, 10, 26]. Ni oxidation behavior without O_2 was studied with *SEI* = 0.46 eV/molecule. The CO_2 conversion is far below 1% when the *SEI* was smaller than 0.5 eV/molecule [72, 73]; in the plasma and thermal oxidation, the CO_2 flow rate, catalyst temperature, and the oxidation time were controlled as 1000 cm^3/min, 600°C, and 70 min, respectively.

After DBD-enhanced oxidation and thermal oxidation, the formation of NiO and its distribution over the cross-section of 3 mm spherical pellet were investigated by Raman spectroscopy and optical microscope. Results showed that the NiO layer was recognized clearly with the thickness of ca. 20 μm. In contrast, the NiO layer was not identified after thermal oxidation. We should point out that the plasma-excited CO_2 has a strong oxidation capability of Ni catalyst. In addition, the effect of DBD is inhibited in the internal pores beyond 20 μm from the pellet surface.

In the thermal oxidation, CO_2 is most likely adsorbed at the perimeter between Ni nanocrystals and Al_2O_3 interfaces [74–76] (**Figure 10(a)**). Subsequently, the adsorbed CO_2 oxidize Ni to NiO near the perimeter. It is clear that the reaction sites for thermal oxidation are limited in the perimeter. The Ni oxidation reaction terminates after the reaction sites are fully oxidized by adsorbed CO_2. In plasma-enhanced oxidation reaction, CO_2 is firstly excited by electron impact. The vibrationally excited CO_2 plays the key role to enhance adsorption process and subsequent oxidation reaction of Ni catalyst, leading to an extensive Ni nanoparticle oxidation, which occurs not only in the perimeter but also in the terrace, step, and kink (**Figure 10(b)**). **Figure 10(c)** and **(d)** show hemispherical catalyst pellets after thermal and plasma oxidation. After thermal oxidation, the external surface and cross-section of catalyst pellets remained black. In contrast, after plasma oxidation, the external surface was oxidized and has showed whitish color change (oxidized stage); in the meantime, the cross-section of the hemispherical pellet has been kept black (unoxidized stage).

The vibrationally excited CO_2 by DBD would induce Ni oxidation to form the oxygen-containing active species (i.e., NiO) rather than simple adsorption, leading to oxygen-rich surface beyond Langmuir isotherm. Incoming plasma-excited CO_2 would carry a few eV internal energy due to the gas phase vibration-to-vibration energy transfer [77, 78], which is the main source of energy for NiO formation. Plasma-excited CO_2 could promote the adsorption flux; however, the adsorbed CO_2 is finally desorbed by the equilibrium limitation unless it forms NiO. In addition, the plasma-induced nonthermal heating mechanism plays another key role in the

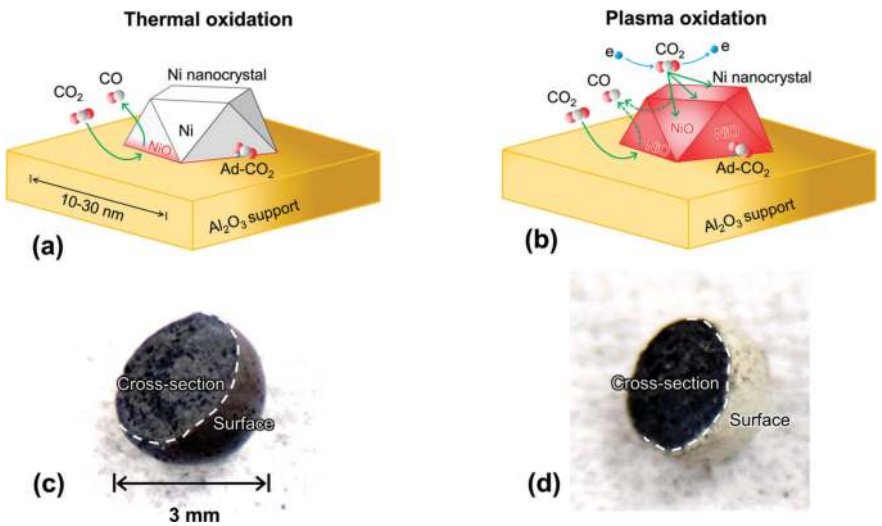

Figure 10.
Ni oxidation pathways: (a) thermal oxidation including CO_2 adsorption near the perimeter of Ni catalysts and (b) plasma-enhanced oxidation. Hemispherical catalyst pellets: (c) thermal oxidation and (d) plasma oxidation.

enhancement of Ni oxidation. Charge recombination and association of radicals can release energy corresponding to 1–10 eV/molecule on catalyst surface. When this excess energy is directly transferred to the adsorbed CO_2, Ni oxidation may be enhanced without increasing macroscopic catalyst temperature. This reaction scheme is explained by nonthermal plasma-mediated Eley-Rideal mechanism, rather than precursor-type adsorption enhancement.

In the DMR process, the oxygen-rich surface (NiO layer) has a capability of oxidizing a large flux of ground-state CH_4 efficiently. Consequently, CH_4 is not necessarily preexcited. CH_4 is almost fully reacted in the NiO layer (20 μm thickness) to inhibit the coke deposition toward the internal pores [26]. However, in the thermal catalysis, NiO is generated in a negligible amount. The ground-state CH_4 can diffuse into internal pores and deposit coke as previously confirmed [26]. Formation of NiO shell (**Figure 10(d)**) and the coke formation behavior (**Figure 9**) are well correlated in plasma catalysis as further discussed in the next section.

5.3 Interaction between DBD and catalyst pores

Although the synergies of plasma and catalyst have been summarized in Section 4, the interaction between DBD and catalyst pores will be further discussed in this section based on the carbon formation and oxidation behavior, as well as DBD-enhanced DMR. For the plasma catalysis, carbon deposition in the internal pores could be remarkably prevented, and fine amorphous carbon filaments were deposited only on the external surface of pellets. A similar trend was observed when NiO was formed in the limited region over the external surface (20 μm depth) only when DBD was superimposed. The results of coke formation behavior and oxidation behavior of Ni-based catalyst in plasma catalysis evidence that the interaction of DBD and catalyst occurs at the external surface of the pellets and the effected thickness is ca. 20 μm. Neither generation of DBD nor diffusion of plasma-generated reactive species in the internal pores is possible. Although DBD and pellet interaction is limited in the external surface, conversion of CH_4 and CO_2 was promoted clearly compared with thermal catalysis: this is the clear evidence of reaction enhancement by DBD.

For DBD, due to the enhanced physical interaction between propagating streamers and catalysts, plasma and catalyst contact area, as well as the streamer propagation from one pellet to the other, are promoted significantly. Nevertheless, electron density in a narrow filamentary channel is of the order of 10^{14} cm^{-3} [6, 79, 80]; in contrast, molecule density at standard condition is approximately 10^{19} cm^{-3}, indicating that a major part of the gas stream is neither ionized nor excited. Consequently, the extremely low proportion of ionized and excited species is inadequate to explain the net increase of CH_4 and CO_2 conversion and selectivity change by DBD. However, if reactive species are fixed and accumulated on the surface of the catalyst, the gross conversion of materials will be promoted. For this reason, the hetero-phase interface between DBD and the external pellet surface provides the most important reaction sites. In Section 5.2, nonthermal plasma oxidation of Ni to NiO creates a critically important step for plasma-enabled synergistic effect.

As Section 4.1 mentioned, gas breakdown is hard to occur in a pore smaller than 10 μm. For the pores catalyst with a pore size less than 2 nm, standard Paschen-type gas breakdown is impossible. To sum up, the external surface of pellet plays the key role for the DBD and catalyst interaction; however, the internal pores play a minor role.

6. Conclusion and outlook

The synergistic effect induced by DBD was clearly observed both in the CH_4 and CO_2 conversion and in the syngas yield. CH_4 dehydrogenation was enhanced by the synergistic effect of DBD and catalyst. Plasma-activated CO_2 and H_2O would promote surface reaction and increase CO and H_2 yield. The analysis of overall activation energy is expected to understand the contribution of plasma-generated reactive species.

In plasma catalysis, the fine amorphous carbon filaments, deposited in the external surface of catalyst, prove that the interaction of DBD occurs mainly in the external surface. The DBD generation and plasma-excited species diffusion are inhibited in the internal pores of the catalyst. Moreover, although the interaction between plasma and catalyst is limited in the external surface, the coke deposition was inhibited significantly in the internal pores by DBD, which is the clear evidence of reaction enhancement by DBD.

Oxidation behavior of Ni-based catalyst in nonthermal plasma-enabled catalysis showed that the NiO layer was generated in the external surface with the thickness of ca. 20 μm during plasma oxidation. In the internal pores, Ni oxidation is inhibited due to the negligible interaction with DBD. Contributing to the NiO layer, the surface of catalyst uptakes more oxygen beyond thermal equilibrium, which is known as Langmuir isotherm, creating a new reaction pathway via NiO. In the plasma catalysis of DMR, NiO drives the oxidation-reduction cycle, which promotes CH_4 dehydrogenation on the surface. Consequently, carbon deposition is suppressed effectively.

For further improvement of plasma-enhanced DMR, the following issues should be investigated:

(1) The effect of radical injection on reaction enhancement should be kinetically analyzed by the Arrhenius plot method, and the analysis of the overall activation energy is expected to understand the contribution of plasma-generated reactive species.

(2) Exploring new types of catalysts, dedicated to plasma catalysis, is an important subject of research. We have demonstrated that the interaction of DBD and catalyst occurs only at the external surface of the pellets, and the effected thickness is ca. 20 μm, which means a majority of the active sites in pores of catalyst do not interact with any excited species. New catalyst preparation method such as catalytic functionalization of reactor wall and catalyst coating for the reactor may be beneficial to strengthen the synergistic effect of nonthermal plasma and catalytically functionalized surface.

(3) The catalyst activity of partially oxidized catalyst and the nonthermal plasma heating mechanism have not been demonstrated experimentally yet; moreover, diagnosis of intermediate species on the surface, created by plasma-derived species, as well as their reaction dynamics are expected to be investigated for deep insight in plasma catalysis.

(4) Although the plasma-induced energy transfer mechanism is commonly accepted in particle growth, it has yet to be investigated within the scope of plasma catalysis. Deep understanding of highly transient and nonequilibrium energy transfer via excited molecules, without macroscopic temperature change, need to be studied.

(5) The individual contribution of radical injection and heat generation, as well as combination of those, must be understood. The gap between macroscopic and microscopic understanding, including various time scales covering nanoseconds to the millisecond, should be bridged by consistent manner.

Author details

Zunrong Sheng, Seigo Kameshima, Kenta Sakata and Tomohiro Nozaki*
Department of Mechanical Engineering, Tokyo Institute of Technology, Tokyo, Japan

*Address all correspondence to: nozaki.t.ab@m.titech.ac.jp

References

[1] Ravanchi MT, Sahebdelfar S. Carbon dioxide capture and utilization in petrochemical industry: Potentials and challenges. Applied Petrochemical Research. 2014;**4**:63-77. DOI: 10.1007/s13203-014-0050-5

[2] Shah YT, Gardner TH. Dry reforming of hydrocarbon feedstocks. Catalysis Reviews. 2014;**56**:476-536. DOI: 10.1080/01614940.2014.946848

[3] Fan MS, Abdullah AZ, Bhatia S. Catalytic technology for carbon dioxide reforming of methane to synthesis gas. ChemCatChem. 2009;**1**:192-208. DOI: 10.1002/cctc.200900025

[4] York APE, Xiao TC, Green MLH, Claridge JB. Methane oxyforming for synthesis gas production. Catalysis Reviews. 2007;**49**:511-560. DOI: 10.1080/01614940701583315

[5] Rostrup-Nielsen JR. New aspects of syngas production and use. Catalysis Today. 2000;**63**:159-164. DOI: 10.1016/S0920-5861(00)00455-7

[6] Kogelschatz U. Dielectric-barrier discharges: Their history, discharge physics, and industrial applications. Plasma Chemistry and Plasma Processing. 2003;**23**(1):1-46. DOI: 10.1023/A:1022470901385

[7] Chang MB, Yu SJ. An atmospheric-pressure plasma process for C_2F_6 removal. Environmental Science & Technology. 2001;**35**:1587-1592. DOI: 10.1021/es001556p

[8] Kameshima S, Tamura K, Mizukami R, Yamazaki T, Nozaki T. Parametric analysis of plasma-assisted pulsed dry methane reforming over Ni/Al_2O_3 catalyst. Plasma Processes and Polymers. 2017;**14**:1600096. DOI: 10.1002/ppap.201600096

[9] Schutze A, Jeong JY, Babayan SE, Jaeyoung P, Selwyn GS, Hicks RF. The atmospheric-pressure plasma jet: A review and comparison to other plasma sources. IEEE Transactions on Plasma Science. 1998;**26**:1685-1694. DOI: 10.1109/27.747887

[10] Kameshima S, Tamura K, Ishibashi Y, Nozaki T. Pulsed dry methane reforming in plasma-enhanced catalytic reaction. Catalysis Today. 2015;**256**:67-75. DOI: 10.1016/j.cattod.2015.05.011

[11] Nozaki T, Okazaki K. Non-thermal plasma catalysis of methane: Principles, energy efficiency, and applications. Catalysis Today. 2013;**211**:29-38. DOI: 10.1016/j.cattod.2013.04.002

[12] Ray D, Reddy PMK, Subrahmanyam C. Ni-Mn/γ-Al_2O_3 assisted plasma dry reforming of methane. Catalysis Today. 2018;**309**:212-218. DOI: 10.1016/j.cattod.2017.07.003

[13] Zeng YX, Wang L, Wu CF, Wang JQ, Shen BX, Tu X. Low temperature reforming of biogas over K-, Mg- and Ce-promoted Ni/Al_2O_3 catalysts for the production of hydrogen rich syngas: Understanding the plasma-catalytic synergy. Applied Catalysis B: Environmental. 2018;**224**:469-478. DOI: 10.1016/j.apcatb.2017.10.017

[14] Tu X, Gallon HJ, Twigg MV, Gorry PA, Whitehead JC. Dry reforming of methane over a Ni/Al_2O_3 catalyst in a coaxial dielectric barrier discharge reactor. Journal of Physics D: Applied Physics. 2011;**44**:274007. DOI: 10.1088/0022-3727/44/27/274007

[15] Van Laer K, Bogaerts A. Influence of gap size and dielectric constant of the packing material on the plasma behaviour in a packed bed DBD reactor: A Fluid Modelling Study. Plasma Processes and Polymers.

2016;**14**:1600129. DOI: 10.1002/ppap.201600129

[16] Michielsen I, Uytdenhouwen Y, Pype J, Michielsen B, Mertens J, Reniers F, et al. CO_2 dissociation in a packed bed DBD reactor: First steps towards a better understanding of plasma catalysis. Chemical Engineering Journal. 2017;**326**:477-488. DOI: 10.1016/j.cej.2017.05.177

[17] Mei D, Tu X. Atmospheric pressure non-thermal plasma activation of CO_2 in a packed-bed dielectric barrier discharge reactor. Chemphyschem. 2017;**18**:3253-3259. DOI: 10.1002/cphc.201700752

[18] Mei D, Tu X. Conversion of CO_2 in a cylindrical dielectric barrier discharge reactor: Effects of plasma processing parameters and reactor design. Journal of CO_2 Utilization. 2017;**19**:68-78. DOI: 10.1016/j.jcou.2017.02.015

[19] Uytdenhouwen Y, Van Alphen S, Michielsen I, Meynen V, Cool P, Bogaerts A. A packed-bed DBD micro plasma reactor for CO_2 dissociation: Does size matter? Chemical Engineering Journal. 2018;**348**:557-568. DOI: 10.1016/j.cej.2018.04.210

[20] Mustafa MF, Fu X, Liu Y, Abbas Y, Wang H, Lu W. Volatile organic compounds (VOCs) removal in non-thermal plasma double dielectric barrier discharge reactor. Journal of Hazardous Materials. 2018;**347**:317-324. DOI: 10.1016/j.jhazmat.2018.01.021

[21] Veerapandian S, Leys C, De Geyter N, Morent R. Abatement of VOCs using packed bed non-thermal plasma reactors: A review. Catalysts. 2017;**7**:113. DOI: 10.3390/catal7040113

[22] Xiao G, Xu W, Wu R, Ni M, Du C, Gao X, et al. Non-thermal plasmas for VOCs abatement. Plasma Chemistry and Plasma Processing. 2014;**34**:1033-1065. DOI: 10.1007/s11090-014-9562-0

[23] Yao S, Shen X, Zhang X, Han J, Wu Z, Tang X, et al. Sustainable removal of particulate matter from diesel engine exhaust at low temperature using a plasma-catalytic method. Chemical Engineering Journal. 2017;**327**:343-350. DOI: 10.1016/j.cej.2017.06.122

[24] Zhu X, Gao X, Qin R, Zeng Y, Qu R, Zheng C, et al. Plasma-catalytic removal of formaldehyde over Cu–Ce catalysts in a dielectric barrier discharge reactor. Applied Catalysis B: Environmental. 2015;**170**:293-300. DOI: 10.1016/j.apcatb.2015.01.032

[25] Patil BS, Cherkasov N, Lang J, Ibhadon AO, Hessel V, Wang Q. Low temperature plasma-catalytic NO_x synthesis in a packed DBD reactor: Effect of support materials and supported active metal oxides. Applied Catalysis B: Environmental. 2016;**194**:123-133. DOI: 10.1016/j.apcatb.2016.04.055

[26] Kameshima S, Mizukami R, Yamazaki T, Prananto LA, Nozaki T. Interfacial reactions between DBD and porous catalyst in dry methane reforming. Journal of Physics D: Applied Physics. 2018;**51**:114006. DOI: 10.1088/1361-6463/aaad7d

[27] Kim HH, Teramoto Y, Negishi N, Ogata A. A multidisciplinary approach to understand the interactions of nonthermal plasma and catalyst: A review. Catalysis Today. 2015;**256**:13-22. DOI: 10.1016/j.cattod.2015.04.009

[28] Du Y, Tamura K, Moore S, Peng Z, Nozaki T, Bruggeman PJ. CO($B^1\Sigma^+ \rightarrow A^1\Pi$) angstrom system for gas temperature measurements in CO_2 containing plasmas. Plasma Chemistry and Plasma Processing. 2017;**37**:29-41. DOI: 10.1007/s11090-016-9759-5

[29] Bröer S, Hammer T. Selective catalytic reduction of nitrogen oxides by combining a non-thermal plasma and a V_2O_5-WO_3/TiO_2 catalyst.

Applied Catalysis B: Environmental. 2000;**28**:101-111. DOI: 10.1016/S0926-3373(00)00166-1

[30] Futamura S, Zhang A, Einaga H, Kabashima H. Involvement of catalyst materials in nonthermal plasma chemical processing of hazardous air pollutants. Catalysis Today. 2002;**72**:259-265. DOI: 10.1016/S0920-5861(01)00503-X

[31] Roland U, Holzer F, Kopinke FD. Improved oxidation of air pollutants in a non-thermal plasma. Catalysis Today. 2002;**73**:315-323. DOI: 10.1016/S0920-5861(02)00015-9

[32] Chang CL, Lin TS. Elimination of carbon monoxide in the gas streams by dielectric barrier discharge systems with Mn catalyst. Plasma Chemistry and Plasma Processing. 2005;**25**:387-401. DOI: 10.1007/s11090-004-3135-6

[33] Van Durme J, Dewulf J, Sysmans W, Leys C, Van Langenhove H. Efficient toluene abatement in indoor air by a plasma catalytic hybrid system. Applied Catalysis B: Environmental. 2007;**74**:161-169. DOI: 10.1016/j.apcatb.2007.02.006

[34] Wallis AE, Whitehead JC, Zhang K. Plasma-assisted catalysis for the destruction of CFC-12 in atmospheric pressure gas streams using TiO_2. Catalysis Letters. 2007;**113**:29-33. DOI: 10.1007/s10562-006-9000-x

[35] Huu TP, Gil S, Da Costa P, Giroir-Fendler A, Khacef A. Plasma-catalytic hybrid reactor: Application to methane removal. Catalysis Today. 2015;**257**:86-92. DOI: 10.1016/j. cattod.2015.03.001

[36] Wang Q, Yan B-H, Jin Y, Cheng Y. Dry reforming of methane in a dielectric barrier discharge reactor with Ni/Al_2O_3 catalyst: Interaction of catalyst and plasma. Energy & Fuels. 2009;**23**:4196-4201. DOI: 10.1021/ef900286j

[37] Kim HH, Tsubota S, Daté M, Ogata A, Futamura S. Catalyst regeneration and activity enhancement of Au/TiO_2 by atmospheric pressure nonthermal plasma. Applied Catalysis A: General. 2007;**329**:93-98. DOI: 10.1016/j.apcata.2007.06.029

[38] Kim HH, Sugasawa M, Hirata H, Teramoto Y, Kosuge K, Negishi N, et al. Ozone-assisted catalysis of toluene with layered ZSM-5 and Ag/ZSM-5 zeolites. Plasma Chemistry and Plasma Processing. 2013;**33**:1083-1098. DOI: 10.1007/s11090-013-9487-z

[39] Chavadej S, Kiatubolpaiboon W, Rangsunvigit P, Sreethawong T. A combined multistage corona discharge and catalytic system for gaseous benzene removal. Journal of Molecular Catalysis A: Chemical. 2007;**263**:128-136. DOI: 10.1016/j.molcata.2006.08.061

[40] Sreethawong T, Thakonpatthanakun P, Chavadej S. Partial oxidation of methane with air for synthesis gas production in a multistage gliding arc discharge system. International Journal of Hydrogen Energy. 2007;**32**:1067-1079. DOI: 10.1016/j.ijhydene.2006.07.013

[41] Harling AM, Glover DJ, Whitehead JC, Zhang K. Novel method for enhancing the destruction of environmental pollutants by the combination of multiple plasma discharges. Environmental Science & Technology. 2008;**42**:4546-4550. DOI: 10.1021/es703213p

[42] Dombrowski E, Peterson E, Del Sesto D, Utz AL. Precursor-mediated reactivity of vibrationally hot molecules: Methane activation on Ir (111). Catalysis Today. 2015;**244**:10-18. DOI: 10.1016/j.cattod.2014.10.025

[43] Nozaki T, Muto N, Kado S, Okazaki K. Dissociation of vibrationally excited methane on Ni catalyst: Part

1. Application to methane steam reforming. Catalysis Today. 2004;**89**: 57-65. DOI: 10.1016/j.cattod.2003.11.040

[44] Nozaki T, Tsukijihara H, Fukui W, Okazaki K. Kinetic analysis of the catalyst and nonthermal plasma hybrid reaction for methane steam reforming. Energy & Fuels. 2007;**21**(5):2525-2530. DOI: 10.1021/ef070117+

[45] Neyts EC. Plasma-surface interactions in plasma catalysis. Plasma Chemistry and Plasma Processing. 2016;**36**:185-212. DOI: 10.1007/s11090-015-9662-5

[46] Chen HL, Lee HM, Chen SH, Chao Y, Chang MB. Review of plasma catalysis on hydrocarbon reforming for hydrogen production—Interaction, integration, and prospects. Applied Catalysis B: Environmental. 2008;**85**:1-9. DOI: 10.1016/j.apcatb.2008.06.021

[47] Van Durme J, Dewulf J, Leys C, Van Langenhove H. Combining non-thermal plasma with heterogeneous catalysis in waste gas treatment: A review. Applied Catalysis B: Environmental. 2008;**78**:324-333. DOI: 10.1016/j.apcatb.2007.09.035

[48] Neyts EC, Bogaerts A. Understanding plasma catalysis through modelling and simulation—A review. Journal of Physics D: Applied Physics. 2014;**47**:224010. DOI: 10.1088/0022-3727/47/22/224010

[49] Vandenbroucke AM, Morent R, De Geyter N, Leys C. Non-thermal plasmas for non-catalytic and catalytic VOC abatement. Journal of Hazardous Materials. 2011;**195**:30-54. DOI: 10.1016/j.jhazmat.2011.08.060

[50] Chang JS, Kostov KG, Urashima K, Yamamoto T, Okayasu Y, Kato T, et al. Removal of NF_3 from semiconductor-process flue gases by tandem packed-bed plasma and adsorbent hybrid systems. IEEE Transactions on Industry Applications. 2000;**36**:1251-1259. DOI: 10.1109/28.871272

[51] Kang WS, Park JM, Kim Y, Hong SH. Numerical study on influences of barrier arrangements on dielectric barrier discharge characteristics. IEEE Transactions on Plasma Science. 2003;**31**:504-510. DOI: 10.1109/TPS.2003.815469

[52] Mizuno A, Ito H. Basic performance of an electrostatically augmented filter consisting of a packed ferroelectric pellet layer. Journal of Electrostatics. 1990;**25**:97-107. DOI: 10.1016/0304-3886(90)90039-X

[53] Mizuno A, Yamazaki Y, Obama S, Suzuki E, Okazaki K. Effect of voltage waveform on partial discharge in ferroelectric pellet layer for gas cleaning. IEEE Transactions on Industry Applications. 1993;**29**:262-267. DOI: 10.1109/28.216530

[54] Kim HH, Teramoto Y, Ogata A. Time-resolved imaging of positive pulsed corona-induced surface streamers on TiO_2 and γ-Al_2O_3-supported Ag catalysts. Journal of Physics D: Applied Physics. 2016;**49**(41):415204. DOI: 10.1088/0022-3727/49/45/459501

[55] Kim HH, Kim JH, Ogata A. Microscopic observation of discharge plasma on the surface of zeolites supported metal nanoparticles. Journal of Physics D: Applied Physics. 2009;**42**:135210. DOI: 10.1088/0022-3727/42/13/135210

[56] Zhang YR, Van Laer K, Neyts EC, Bogaerts A. Can plasma be formed in catalyst pores? A modeling investigation. Applied Catalysis B: Environmental. 2016;**185**:56-67. DOI: 10.1016/j.apcatb.2015.12.009

[57] Hensel K, Martišovitš V, Machala Z, Janda M, Leštinský M, Tardiveau P, et al. Electrical and optical properties of AC microdischarges in porous ceramics. Plasma Processes and Polymers. 2007;**4**:682-693. DOI: 10.1002/ppap.200700022

[58] Wang Z, Zhang Y, Neyts EC, Cao X, Zhang X, Jang BWL, et al. Catalyst preparation with plasmas: How does it work? ACS Catalysis. 2018;**8**:2093-2110. DOI: 10.1021/acscatal.7b03723

[59] Blin-Simiand N, Tardiveau P, Risacher A, Jorand F, Pasquiers S. Removal of 2-heptanone by dielectric barrier discharges—The effect of a catalyst support. Plasma Processes and Polymers. 2005;**2**:256-262. DOI: 10.1002/ppap.200400088

[60] Liu C, Zou J, Yu K, Cheng D, Han Y, Zhan J, et al. Plasma application for more environmentally friendly catalyst preparation. Pure and Applied Chemistry. 2006;**78**:1227-1238. DOI: 10.1351/pac200678061227

[61] Hong J, Chu W, Chernavskii PA, Khodakov AY. Cobalt species and cobalt-support interaction in glow discharge plasma-assisted Fischer-Tropsch catalysts. Journal of Catalysis. 2010;**273**:9-17. DOI: 10.1016/j.jcat.2010.04.015

[62] Shang S, Liu G, Chai X, Tao X, Li X, Bai M, et al. Research on Ni/γ-Al_2O_3 catalyst for CO_2 reforming of CH_4 prepared by atmospheric pressure glow discharge plasma jet. Catalysis Today. 2009;**148**:268-274. DOI: 10.1016/j.cattod.2009.09.011

[63] Wang L, Zhao Y, Liu C, Gong W, Guo H. Plasma driven ammonia decomposition on a Fe-catalyst: Eliminating surface nitrogen poisoning. Chemical Communications. 2013;**49**:3787-3789. DOI: 10.1039/C3CC41301B

[64] Smith RR, Killelea DR, DelSesto DF, Utz AL. Preference for vibrational over translational energy in a gas-surface reaction. Science. 2004;**304**:992-995. DOI: 10.1126/science.1096309

[65] Demidyuk V, Whitehead JC. Influence of temperature on gas-phase toluene decomposition in plasma-catalytic system. Plasma Chemistry and Plasma Processing. 2007;**27**:85-94. DOI: 10.1007/s11090-006-9045-z

[66] Nozaki T, Okazaki K. Carbon nanotube synthesis in atmospheric pressure glow discharge: A review. Plasma Processes and Polymers. 2008;**5**:300-321. DOI: 10.1002/ppap.200700141

[67] Nozaki T, Fukui W, Okazaki K. Reaction enhancement mechanism of the nonthermal discharge and catalyst hybrid reaction for methane reforming. Energy & Fuels. 2008;**22**:3600-3604. DOI: 10.1021/ef800461k

[68] Mutz B, Carvalho HWP, Mangold S, Kleist W, Grunwaldt JD. Methanation of CO_2: Structural response of a Ni-based catalyst under fluctuating reaction conditions unraveled by operando spectroscopy. Journal of Catalysis. 2015;**327**:48-53. DOI: 10.1016/j.jcat.2015.04.006

[69] Mutz B, Carvalho HWP, Kleist W, Grunwaldt JD. Dynamic transformation of small Ni particles during methanation of CO_2 under fluctuating reaction conditions monitored by operando X-ray absorption spectroscopy. Journal of Physics: Conference Series. 2016;**712**:012050. DOI: 10.1088/1742-6596/712/1/012050

[70] Snoeckx R, Bogaerts A. Plasma technology—A novel solution for CO_2 conversion? Chemical Society Reviews. 2017;**46**:5805-5863. DOI: 10.1039/C6CS00066E

[71] Belov I, Vanneste J, Aghaee M, Paulussen S, Bogaerts A. Synthesis of micro- and nanomaterials in CO_2 and CO dielectric barrier discharges. Plasma Processes and Polymers. 2016;**14**:1600065. DOI: 10.1002/ppap.201600065

[72] Aerts R, Somers W, Bogaerts A. Carbon dioxide splitting in a dielectric

barrier discharge plasma: A combined experimental and computational study. ChemSusChem. 2015;**8**:702-716. DOI: 10.1002/cssc.201402818

[73] Butterworth T, Elder R, Allen R. Effects of particle size on CO_2 reduction and discharge characteristics in a packed bed plasma reactor. Chemical Engineering Journal. 2016;**293**:55-67. DOI: 10.1016/j.cej.2016.02.047

[74] Mutz B, Gänzler MA, Nachtegaal M, Müller O, Frahm R, Kleist W, et al. Surface oxidation of supported Ni particles and its impact on the catalytic performance during dynamically operated methanation of CO_2. Catalysts. 2017;**7**:279. DOI: 10.3390/catal7090279

[75] Foppa L, Margossian T, Kim SM, Müller C, Copéret C, Larmier K, et al. Contrasting the role of Ni/Al_2O_3 interfaces in water–gas shift and dry reforming of methane. Journal of the American Chemical Society. 2017;**139**:17128-17139. DOI: 10.1021/jacs.7b08984

[76] Silaghi MC, Comas-Vives A, Copéret C. CO_2 activation on Ni/γ-Al_2O_3 catalysts by first-principles calculations: From ideal surfaces to supported nanoparticles. ACS Catalysis. 2016;**6**:4501-4505. DOI: 10.1021/acscatal.6b00822

[77] Bogaerts A, Kozák T, van Laer K, Snoeckx R. Plasma-based conversion of CO_2: Current status and future challenges. Faraday Discussions. 2015;**183**:217-232. DOI: 10.1039/C5FD00053J

[78] Van Rooij GJ, van den Bekerom DCM, den Harder N, Minea T, Berden G, Bongers WA, et al. Taming microwave plasma to beat thermodynamics in CO_2 dissociation. Faraday Discussions. 2015;**183**:233-248. DOI: 10.1039/C5FD00045A

[79] Nozaki T, Miyazaki Y, Unno Y, Okazaki K. Energy distribution and heat transfer mechanisms in atmospheric pressure non-equilibrium plasmas. Journal of Physics D: Applied Physics. 2001;**34**:3383

[80] Nozaki T, Unno Y, Okazaki K. Thermal structure of atmospheric pressure non-equilibrium plasmas. Plasma Sources Science and Technology. 2002;**11**:431. DOI: 10.1088/0963-0252/11/4/310